

Unexpected Dynamical Instabilities In Differentially Rotating Neutron Stars

Shangli Ou and Joel E. Tohline

*Department of Physics & Astronomy, Center for Computation & Technology,
Louisiana State University, Baton Rouge, LA 70803*

ABSTRACT

A one-armed spiral instability has been found to develop in differentially rotating stellar models that have a relatively stiff, $n = 1$ polytropic equation of state and a wide range of rotational energies. This suggests that such instabilities can arise in neutron stars that are differentially, although not necessarily rapidly, rotating. The instability seems to be directly triggered by the presence of a corotation resonance inside the star. Our analysis also suggests that a resonant cavity resulting from a local minimum in the radial vortensity profile of the star plays an important role in amplifying the unstable mode. Hence, it appears as though this instability is closely related to the so-called “Rossby wave instability” (Lovelace et al. 1999) that has been found to arise in accretion disks. In addition to the one-armed ($m = 1$) spiral mode, we have found that higher-order ($m = 2$ and $m = 3$) nonaxisymmetric modes also can become unstable if corotation points that resonate with the eigenfrequencies of these higher-order modes also appear inside the star. The growth rate of each mode seems to depend on the location of its corotation radius with respect to the vortensity profile (or on the depth of its corotation radius inside the vortensity well). The existence of such instabilities makes the stability criterion for differentially rotating neutron stars non-unique. Also, the gravitational-waves emitted from such unstable systems generally will not have a monochromatic frequency spectrum.

Subject headings: neutron stars — one-armed instabilities — corotation — differential rotation — vortensity — Rossby wave instability — gravitational waves

1. Introduction

Rotating stars are subject to a variety of nonaxisymmetric instabilities (Chandrasekhar 1969; Tassoul 1978; Andersson 2003). If a star rotates sufficiently fast – to a point where the

ratio of its rotational to gravitational potential energy $T/|W| \gtrsim 0.27$ – it will encounter a dynamical bar-mode instability that will result in the deformation of the star into a rapidly spinning, bar-like structure. This instability has been verified by a number of numerical hydrodynamics investigations (Tohline, Durisen, & McCollough 1985; Durisen et al. 1986; Williams & Tohline 1988; Cazes & Tohline 2000; New, Centrella & Tohline 2000; Brown 2000; Liu 2002). At a slower rotation rate, $T/|W| \gtrsim 0.14$, a star may also encounter a secular bar-mode instability that can promote deformation into a bar-like shape, but only if the star is subjected to a dissipative process capable of redistributing angular momentum within its structure, such as viscosity or gravitational radiation reaction (GRR) forces (Chandrasekhar 1970; Friedman & Schutz 1978; Ipser & Lindblom 1990, 1991; Lai & Shapiro 1995). In reality, viscosity and GRR forces tend to compete with each other and can drive the secularly unstable star along a variety of different evolutionary paths. Recently, Shibata & Karino (2004) and Ou, Tohline & Lindblom (2004) used numerical hydrodynamic techniques to study the nonlinear evolution of the GRR-driven secular bar-mode instability in rotating, “polytropic” neutron stars in the absence of any competing dissipation. The above studies have shown that the critical limits of both the secular and dynamical bar-mode instabilities do not depend sensitively on the degree of compressibility of the equation of state (EOS) or on the differential rotation law of a star.

Surprisingly, several recent numerical studies have found that dynamical instabilities that excite $m = 1$ as well as $m = 2$ azimuthal Fourier modes can arise in self-gravitating structures having $T/|W| < 0.27$, that is, having a rotational energy below the threshold traditionally expected for dynamical nonaxisymmetric instabilities. Tohline & Hachisu (1990) found an $m = 2$ instability in self-gravitating rings and tori having uniform specific angular momentum and $T/|W| \gtrsim 0.16$. Centrella et al. (2001) found a one-armed ($m = 1$) spiral instability in stellar models with a polytropic index $n = 3.33$, strong differential rotation and $T/|W| \sim 0.14$. Shibata et al. (2002, 2003) found an $m = 2$ instability in extremely differentially rotating stellar models having $T/|W|$ on the order of 10^{-2} ! Saijo et al. (2003) concluded that one-armed ($m = 1$) modes only appear in structures with a very soft equation of state ($n \gtrsim 2.5$), and that a necessary condition for this instability to arise is the presence of an off-center density maximum, that is, a toroidal-like structure. Ott et al. (2005a) showed that a one-armed spiral instability may arise in the context of a pre-supernova core collapse. The linear analysis of Watts et al. (2004) has suggested that these low $T/|W|$ instabilities are triggered because corotation points of the unstable modes fall within the differentially rotating structure of the examined models. Saijo & Yoshida (2005) also have carried out a linear stability analysis that shows a connection between the one-armed, $m = 1$ instability and corotation points in differentially rotating stars.

Many earlier studies of disks and tori have also noted an association between the onset

of dynamical instabilities and the existence of corotation points. For example, a number of groups (Papaloizou & Pringle 1984; Goldreich, Goodman, & Narayan 1986; Narayan, Goldreich, & Goodman 1987; Frank & Robertson 1988) have used both linear analyses and nonlinear simulations to study the so-called Papaloizou-Pringle instability, which is triggered by corotation resonances. But the existence of a corotation point within a model is not sufficient to ensure significant growth of an unstable mode. It appears as though a resonant cavity is also required to drive these modes to very large amplitude. In the case of the Papaloizou-Pringle instability, the inner and outer edges of the disk or torus form a resonant cavity in which waves are reflected back and forth; the unstable mode is greatly amplified through multiple passages across the corotation radius. However, it is not obvious how such a resonant cavity can exist in stellar models that have no inner edges.

Lovelace & Hohlfield (1978) and Papaloizou & Lin (1989) have discussed how the radial distribution of vortensity or potential vorticity, which is defined as the ratio between vorticity and surface density, is important in determining the stability of homentropic, self-gravitating rings and disks. Lovelace et al. (1999) and Li et al. (2000) extended this discussion to non-homentropic disks. According to their analysis of the so-called “Rossby-Wave Instability”, local minima in the radial vortensity profile of homentropic configurations tend to trap radially propagating waves and, hence, can serve as resonant cavities that will help drive corotation instabilities to large amplitude. This removes the necessity of having disk edges to serve as reflecting boundaries. In their subsequent nonlinear simulations, Li et al. (2001) found that this mechanism can aid in the excitation of nonaxisymmetric instabilities ($m = 1, 3, 5$) and vortex formation in accretion disks. It is interesting to note that when the initial perturbations in these nonlinear simulations contained the pure eigenfunctions for a given azimuthal mode (for example, $m = 3$ or 5), the corresponding mode developed; but, when a white noise initial perturbation was used, an $m = 1$ spiral mode became dominant in the final stage.

It is conceivable that a similar resonant cavity mechanism may work to amplify corotation resonances in stellar models. This would seem to be especially likely for rapidly rotating models that have toroidal-like structures because the associated off-center density maximum will inevitably result in a dip in the radial vortensity profile of the star. This profile could then act as a resonant cavity to trap radially propagating waves. Alternatively, a maximum in the star’s radial entropy profile can also produce such a cavity (Lovelace et al. 1999), but in keeping with most previous studies of the low $T/|W|$ instabilities we will confine our analysis to homentropic configurations where a dip in the vortensity profile will be required to create a resonant cavity.

In this paper, we report the unexpected discovery of an $m = 1$ spiral-mode instability in

rotating stars with a relatively stiff ($n = 1$) polytropic EOS that was designed to represent differentially rotating neutron stars. We also show evidence that this instability is directly triggered by the existence inside the star of a corotation radius for the eigenmode. This one-armed spiral instability develops on a timescale that is somewhat longer than the growth time observed in previous studies of configurations with a softer EOS, but the instability appears to be dynamical nevertheless. All of our unstable models exhibit a local minimum in their radial vortensity profile and this seems likely to be the resonant cavity that traps the wave and permits it to amplify. (We have found that such a minimum can exist in configurations with centrally condensed, rather than toroidal, density structures when the degree of differential rotation is sufficiently strong.) Our results suggest that it is the combination of corotation points and resonant cavities formed by vortensity minima that is responsible for the excitation of low $T/|W|$ instabilities found in stellar models.

Perhaps our most striking discovery is that, in addition to the $m = 1$ mode, $m=2$ and 3 modes also come into play as long as their corotation points exist within the structure of the star. Therefore, if the rotational profile of the star is steep enough to contain corotation points of multiple modes, these unstable modes may all arise within one single star. The entire picture of rotational instabilities that might arise in differentially rotating neutron stars becomes more complicated due to the co-existence of these corotation instabilities. The corresponding gravitational-wave signals may exhibit different characteristic frequencies at different or overlapping times, since various unstable modes may set in simultaneously.

2. Initial Models and Numerical Methods

2.1. Initial Axisymmetric Models

Using the Hachisu self-consistent-field technique (Hachisu 1986), four simplified axisymmetric neutron star models (models **J250**, **J133**, **J127**, and **J068**) were constructed on a cylindrical grid with resolution $66 \times 82 \times 128$ in the radial, vertical and azimuthal directions, respectively. For each model, we have adopted a dimensionless unit system in which the gravitational constant G , the maximum density ρ_{\max} , and the radius of the entire grid R_{grid} are set to 1. For comparison purposes, equatorial radii R_{eq} were all set to 0.673. All the models were constructed using Newtonian gravity and a polytropic equation of state, $p = K\rho^{1+1/n}$, where p is the gas pressure, K is a polytropic constant, and the polytropic index n was in all cases chosen to be 1. The angular velocity profiles were specified by the so-called j-constant-like law as,

$$\Omega(R) = \frac{\omega_c A^2}{R^2 + A^2}, \quad (1)$$

where $R = \sqrt{x^2 + y^2}$ is the cylindrical radius, A is a constant, and ω_c is the angular velocity at the rotation axis (the Z-axis). The specific parameter values of each model are given in Table 1, where $\bar{\rho}$ is the mean density of the star, ρ_c is the central density (which will be less than ρ_{\max} if the model exhibits an off-center density maximum), and R_p is the polar radius.

2.2. Analysis Method

We used a three-dimensional (3D), Newtonian hydrodynamics code essentially the same as the one employed by Ou, Tohline & Lindblom (2004, hereafter Paper I) to study the evolution of our differentially rotating, neutron stars models. The details of the hydrodynamics code can be found in Motl, Tohline, & Frank (2002). In paper I, an artificially enhanced gravitational-radiation-reaction (GRR) potential was introduced into the code to mimic the GRR effect, which will induce the secular bar-mode instability when the $T/|W|$ value of the star exceeds the critical limit 0.14.

In order to monitor the growth of nonaxisymmetric modes, we measured the Fourier amplitude of each mode with azimuthal quantum number m in the following fashion: At any point in time during an evolution, the azimuthal density distribution in a ring of fixed R and z can be decomposed into a series of azimuthal Fourier components via the relation,

$$\rho(R, z, \phi) = \sum_{m=-\infty}^{+\infty} C_m(R, z)e^{im\phi}, \quad (2)$$

where the complex amplitudes C_m are defined by the expression,

$$C_m(R, z) = \frac{1}{2\pi} \int_0^{2\pi} \rho(R, z, \phi)e^{-im\phi} d\phi. \quad (3)$$

In our simulations, the time-dependent behavior of the magnitude of this coefficient, $|C_m|$, is then monitored to measure the growth-rate of various unstable modes. At any point in time, the ratio between the imaginary and real parts of $C_m(R, z)$ gives us a spatially dependent phase angle $\phi_m(R, z)$ from which we also are able to determine the azimuthal structure of each unstable mode m , if it exists. (In particular, the radial dependence of ϕ_m tells us, for example, whether an $m = 1$ mode has a spiral character or an $m = 2$ mode has a bar-like structure; see Figures 14 and 15, below.) In general, $\phi_m(R, z)$ is a function of time, but an eigenmode of the system becomes identifiable when the spatial structure of the phase angle $\phi_m(R, z)$ appears to be coherent/aligned throughout the star and time-independent, apart from a spatially independent azimuthal eigenfrequency $\omega_m \equiv \partial\phi_m/\partial t$ of the mode. Another way to look at this is that the oscillation period of mode m , $T_m \equiv 2\pi/\omega_m$, is

equivalent to the time it takes the real or imaginary parts of C_m to complete a full cycle from a positive value to a negative value, then back to a positive value. In our nonlinear hydrodynamic simulations, the measurement of ω_m is accurate only when the corresponding mode dominates the evolution.

By definition, the corotation radius R_{cor} of mode m is the radial location in the star where the angular velocity of the fluid resonates with the eigenfrequency of the unstable mode, that is, where $\omega(R_{\text{cor}}) = \omega_m/m$. In our analysis, we also will find it useful to refer to each model’s central spin period, $T_c = 2\pi/\omega_c$, and characteristic dynamical time scale, $T_0 \equiv 2\pi/\omega_0$, where $\omega_0 \equiv \sqrt{\pi G \bar{\rho}}$.

3. Simulation Results

In this section, we show results from a number of independent 3D hydrodynamic evolutions. Because our initial goal was to study the secular bar-mode instability induced by GRR forces, rather than the development of a one-armed spiral instability, the initially axisymmetric density structure of all models was perturbed with an $m = 2$ perturbation with different amplitude as they were introduced into the hydrodynamics code. In the discussion that follows, the evolution time of individual simulations has been normalized to the spin period at the rotation axis of each star T_c , which varies significantly for different models, but in terms of the characteristic dynamical time, T_0 , they were evolved for roughly the same times, except for model **J127**. Table 2 summarizes all the relevant frequencies and time scales for each of our models. In addition to the time scales and frequencies defined earlier, τ_m is the measured e-folding (growth) time for a given mode m , and ω_s is the angular frequency at the equatorial surface. We note that, for a given model, the eigenfrequencies quoted in Table 2 have been measured at different evolutionary times. Each ω_m is measured at a time when the corresponding mode m is dominant, and the corresponding corotation radius is determined from the system’s equatorial plane rotational profile at that same time.

3.1. Evolution of model J250

This investigation began as an extension of Paper I (where uniformly rotating neutron stars were studied) and our initial aim was to study the secular bar-mode instability in differentially rotating neutron stars. The first model we evolved was model **J250**, which was expected to be secularly unstable but dynamically stable to the high $T/|W|$ bar-mode instability. Because the model had a relatively large value of the parameter A , it also

Table 1. Parameters of Initial Models

Model	n	A/R_{eq}	R_p/R_{eq}	M_{tot}	ρ_c/ρ_{max}	$\bar{\rho}$	ω_c	$T/ W $	unstable modes
J250	1.0	0.94	0.302	0.204	0.976	0.384	1.44	0.250	m=1
J133	1.0	0.94	0.558	0.257	0.999	0.309	1.19	0.133	-
J127	1.0	0.59	0.558	0.335	0.999	0.363	1.75	0.127	m=1,2,3
J068	1.0	0.44	0.721	0.384	1.000	0.343	1.80	0.068	m=1,2

Note. — n is polytropic index, A is a parameter that determines the degree of differential rotation, R_{eq} is the equatorial radius, R_p is the polar radius, M_{tot} is the total mass, ρ_c is the central density, ρ_{max} is the maximum density, $\bar{\rho}$ is the mean density, ω_c is the angular frequency at the center, T is the rotational energy, W is the gravitational energy.

Table 2. Relevant Frequencies of All Models

Model	ω_c	ω_s	$\omega_0 = \sqrt{\pi G \bar{\rho}}$	ω_1	$\omega_2/2$	$\omega_3/3$	τ_1/T_0	τ_2/T_0	τ_3/T_0
J250	1.44	0.66	1.10	1.2	-	-	9.4	-	-
J133	1.19	0.54	0.98	-	-	-	-	-	-
J127	1.75	0.44	1.07	1.3	0.9	1.0	29.4	7.8	4.2
J068	1.80	0.29	1.04	1.3	0.9	-	8.4	4.4	-

Note. — ω_c is the angular frequency at the center, ω_s is the angular frequency at the equatorial surface, $\bar{\rho}$ is the mean density, ω_m is the eigenfrequency of the azimuthal mode m , τ_m is the e-folding time of the azimuthal mode m , $T_0 = 2\pi/\omega_0$. As illustrated in Figure 9, for a given model, the eigenfrequencies ω_m have been measured at different evolutionary times, when each mode dominates.

was expected to be stable to the low $T/|W|$ dynamical bar-mode instability identified by Shibata et al. (2002). Model **J250** was evolved for many dynamical times with an artificially enhanced GRR potential, in a manner similar to the evolutions described in Paper I.

The top panel of Figure 1 shows the time-evolution of the amplitudes of different modes (averaged over the whole volume) throughout this evolution. In the beginning, the $m = 2$ bar-mode grows exponentially on a timescale governed by the artificially enhanced GRR potential; but it saturates after only a moderately deformed bar structure has formed. This is consistent with the results reported by Shibata & Karino (2004). However, on a considerably longer time scale, an unexpected $m = 1$ mode arises and becomes the dominant mode. The density contour plots in the bottom right-hand panel of Figure 1 suggest that the $m = 1$ mode has a one-armed spiral structure similar to the one discovered by Centrella et al. (2001). We note that, late in the evolution, the amplitude of the $m = 2$ mode increases when the $m = 1$ mode reaches the nonlinear regime. (This feature is common to all of our models that are unstable to the $m = 1$ mode.) Measurements of ω_m for various modes at the time when the $m = 1$ mode is dominant confirms that, for example, $\omega_2 \approx 2\omega_1 \approx 2.6$ and suggests that, at late times, the $m = 2$ mode is a harmonic of the $m = 1$ mode.

This discovery is unexpected in the sense that the one-armed, $m = 1$ instability had previously appeared only in models with a softer EOS ($n \gtrsim 2.5$) and with a high degree of differential rotation, i.e., $\omega_c/\omega_s \approx 10$ (Centrella et al. 2001; Saijo et al. 2003; Saijo & Yoshida 2005), where ω_s is the angular frequency at the equatorial surface. In contrast, our model **J250** has an $n = 1$ polytropic EOS and has only a moderate degree of differential rotation with $\omega_c/\omega_s \approx 2$.

In order to test whether or not this instability was caused by the artificially enhanced GRR forces, a second evolution was performed on model **J250** with GRR turned off. Figure 2 shows the time-evolution of the amplitudes of different modes for this second evolution. As expected, the $m = 2$ bar-mode was not unstable in the absence of GRR forces, but surprisingly the $m = 1$ mode remained unstable, becoming the dominant Fourier component at time $\gtrsim 100 T_c$. Compared to models that had a softer EOS (Centrella et al. 2001; Saijo et al. 2003) in which the $m = 1$ mode grew on a time scale of a few tens of T_c , the growth time here is much longer but nevertheless still dynamical. (We note that the growth time in this pure hydrodynamical evolution is also longer than that from the previous run, in which GRR was turned on. This is probably because GRR tends to increase the degree of differential rotation, hence influence the growth rate of the $m = 1$ mode.) The top panel of Figure 3 shows the radial eigenfunction of the $m = 1$ mode obtained by subtracting the initial axisymmetric background density (bottom panel of Figure 3). Its behavior is qualitatively similar to that derived from a linear stability analysis by Saijo & Yoshida (2005) (see their

Figure 9).

The appearance of the one-armed spiral instability in our models with a stiff EOS seems to suggest that its stability criterion is independent of compressibility. Now the question is what mechanism is responsible for its growth? According to Watts et al. (2004), Saijo & Yoshida (2005), and related studies of disks and tori (Papaloizou & Pringle 1984; Goldreich, Goodman, & Narayan 1986; Narayan, Goldreich, & Goodman 1987), corotation points may be responsible for the amplification of some unstable modes. But this mechanism of amplification can only operate if there is at least one radial location in the model where the angular frequency of orbiting fluid elements resonates with the eigenfrequency of the identified special mode. A straightforward check of the radial rotational profiles $\Omega(R)$ of model **J250** (see Figure 4) shows that a corotation radius is present at $R \approx 0.32$ for the unstable $m = 1$ Fourier mode with an eigenfrequency $\omega_1 \approx 1.2$. (This measurement of the eigenfrequency was done for the pure hydrodynamical simulation, in which GRR was turned off.)

However, the result from one model is not sufficient for us to draw a definite conclusion. To further clarify the relationship between the instability and corotation points, we performed a number of simulations on different polytropic neutron star models. In these additional simulations, we will concentrate only on hydrodynamic simulations with GRR turned off, because GRR-related instabilities generally would set in on a much longer time scale and therefore are irrelevant here.

3.2. Evolution of model **J133**

So far we have identified a corotation point associated with the one-armed spiral instability in model **J250**. It would be interesting to find out if the instability disappears when there is no such corotation point. In order to test this, we chose to evolve model **J133**. This model is rotating slowly enough so that the central angular frequency is well below the eigenfrequency of the $m = 1$ mode that arose in model **J250**. By removing the corotation points of the $m = 1$ mode inside model **J133**, it was hoped that the one-armed instability would not show up in this evolution. To eliminate the possible influence of the degree of differential rotation, we kept the value of the parameter A the same as in model **J250**, but increased the polar radius R_p to slow down the rotation of the star. Note that the eigenfrequency of the $m = 1$ mode for this model is actually unknown¹, but we estimate it would not change

¹Our studies do not include a method for performing a complete eigenmode analysis of our selected, initially axisymmetric models. Only modes that are unstable and that grow on a timescale short compared

dramatically compared to that of model **J250**. (In fact, as shown by later simulations, ω_1 in model **J250** and **J127** are very close to each other; see Table 2.)

As shown in the top panel of Figure 5, the $m = 1$ Fourier amplitude $|C_1|$ does not grow into the nonlinear regime in this case. It develops somewhat, but only hangs on at a very small amplitude. On the other hand, the $m = 2$ mode seems to gain some strength in the beginning of the evolution, but it quickly saturates at a very low amplitude and never enters into the nonlinear regime. The density contours shown in the bottom panels of Figure 5 also display no indication of nonaxisymmetric structure. The lack of development of the $m = 1$ spiral mode in this simulation supports our conjecture that corotation points are directly responsible for the excitation of the mode.

3.3. Evolution of model **J127**

Although the evolution of model **J133** makes our argument about corotation points plausible, the fact that its $T/|W|$ value is significantly lower than model **J250** raised the following question: is it the low $T/|W|$ value that suppressed the instability? To answer this question and as a further check of our conjecture, model **J127** was evolved in the same fashion as model **J133**. This model has a $T/|W|$ value that is similar to that of model **J133**, but its degree of differential rotation was made very high by reducing the value of A . With this steep rotational profile, we hoped that a corotation point for the $m = 1$ mode would exist within the star and, hence, trigger the instability.

The final outcome of this evolution is perhaps the most striking and interesting one. As shown in the top panel of Figure 6, the evolution can be divided into three stages: (1) In the first $\sim 50 T_c$, an $m = 2$ mode grows exponentially, but it saturates very quickly; (2) $\sim 30 T_c$ later, an unexpected $m = 3$ mode comes into play, and becomes dominant for quite a long time. The pear-shaped $m = 3$ density distortion is visible in the bottom left-hand panel of Figure 6; (3) after $\approx 300T_c$, the originally expected $m = 1$ mode catches up and wins over.

Given previous studies of the low $T/|W|$ bar-mode instability (Shibata et al. 2002), the appearance of the $m = 2$ mode here is not surprising. However, the appearance of an $m = 3$ mode in axisymmetric equilibrium stellar models with intermediate $T/|W|$ values is totally unexpected. A plot of the rotational profile of model **J127** is shown in Figure 7 and reveals the existence of corotation radii for all three of these unstable modes. These results are fully consistent with the linear analysis presented by Watts et al. (2004): Corotation instabilities

to our evolution times can be identified using our present nonlinear hydrodynamic tools.

in stellar models are not limited to $m = 1$ and $m = 2$ modes. Other modes may become unstable as long as their corotation points exist inside the star. In this simulation, we also analyzed the behavior of the $m = 4$ (5) Fourier component of the density distribution. It appears to follow the behavior of the $m = 2$ (3) mode, but it saturates at an amplitude that is two orders of magnitude lower. This suggests that the $m = 4$ (5) “mode” is actually a harmonic of $m = 2$ (3). There is no indication of the independent development of either an $m = 4$ or 5 mode. We suspect that the reason for the lack of independent $m=4$ and 5 modes is that their corotation radii fall outside the star.

Because instabilities associated with different modes may arise in stars with strong differential rotation, the gravitational-wave signals from such an event would exhibit multiple characteristics. Figure 8 shows the computed quadrupole gravitational-wave strain as viewed by an observer located along the $+Z$ axis and assuming the neutron star has a mass of $1.4 M_{\odot}$ and an equatorial radius of 12.5 km. The peak signal strength is actually stronger than the bounce signal expected from the axisymmetric core collapse of massive stars, which has been shown to produce signals with $rh_+ \approx 300$ cm at a frequency $f \approx 400$ Hz (Ott et al. 2004). The signal also has some distinct features. There is more than one localized burst, arising from different modes peaking at different times and in different frequency bands: the first, centered at $t/T_c \sim 65$, corresponds to $rh_+ \sim 500$ cm at a frequency $f \approx 1800$ Hz emitted by the $m = 2$ mode; the second, centered at $t/T_c \sim 100$, corresponds to $rh_+ \sim 600$ cm at a frequency $f \approx 1900$ Hz associated with the $m = 3$ mode; the third, centered at $t/T_c \sim 375$, corresponds to a $rh_+ \sim 900$ cm at frequency $f \approx 2600$ Hz emitted by the $m = 2$ harmonic of the $m = 1$ spiral mode.

Figure 9 shows the pattern frequencies of all the dominating unstable modes as a function of time. To make the graph clean, the frequencies of the $m = 1$ and 2 modes are only shown in the time intervals when they dominate, and all the data at times $t < 40T_c$ have been omitted because they appear to be noisy due to the lack of coherent modes. It is observed that the pattern frequencies of all three modes – $\omega_1, \omega_2/2$, and $\omega_3/3$ – are fairly constant throughout their period of dominance and the uncertainty in these measurements is $\lesssim 10\%$. Hence, the relative location of the corotation radii R_{cor} for these various modes does not vary with time, unless a change in the rotational profile of the star causes R_{cor} to migrate.

Based upon the above hydrodynamic simulations, we can now draw the following conclusions: (1) The $m = 1$ instability can be turned on or off by controlling the rotational profile of the star to allow or remove the existence of a corotation point. (2) The instability is not limited to the $m = 1$ mode; other modes may also arise, as long as their corotation points exist inside the star.

3.4. Evolution of model J068

According to Shibata et al. (2002, 2003), models with very small values of the rotation-profile parameter A are subject to a low $T/|W|$ dynamical bar-mode instability. Since the rotational profiles for these types of models are quite steep, it occurred to us that they may also allow corotation points for various modes within their structure. It also seemed likely that even one individual stellar model might be subject to instabilities associated not only with the $m = 2$ bar-mode, but also other modes. In order to test this idea, we evolved model **J068** with $A/R_{eq} = 0.44$ ($\omega_c/\omega_s \approx 6$), which falls in the instability region where the low $T/|W|$ dynamical bar-mode instability would be expected to set in.

The results of this simulation support our suspicion that an individual model with a very steep rotational profile may be subject to multiple instabilities associated with different azimuthal modes. As shown in the top panel of Figure 10, at the beginning of this simulation the $m = 2$ bar-mode grew very quickly, became nonlinear, and dominated the evolution for quite a while, which is consistent with the results presented by Shibata et al. (2002). In addition, however, we found that the underlying $m = 1$ and 3 modes also grew simultaneously. These odd-numbered modes had growth rates rather slower than the $m = 2$ mode, but this did not keep the $m = 1$ mode from finally winning over all the other modes, including the bar-mode, and manifesting itself as the dominant mode, just as it did in our earlier simulations. Notice that, again, the amplitude of the $m = 2$ mode increases when the $m = 1$ mode becomes dominant at late times, which suggests that the $m = 2$ mode is a harmonic of the $m = 1$ mode during this period.

The rotational profile of model **J068**, shown in Figure 11, reveals corotation points for both $m = 1$ and 2 modes. (We could not accurately measure the eigenfrequency of the $m = 3$ mode because it never became the dominant mode in the evolution time followed by our simulation.)

4. Summary and Discussion

We have found that a one-armed spiral instability arises in rotating $n = 1$ “polytropic” neutron stars with moderate and high degrees of differential rotation. This is in contrast to the work of Saijo et al. (2003), which has suggested that such instabilities can arise only in stars with a softer EOS. As has been suggested by Saijo & Yoshida (2005), the instability seems to be associated with the existence of a corotation point of the $m = 1$ mode that lies inside the star. Given previous results for models with a softer EOS, we conclude that the compressibility and $T/|W|$ value of the star are not directly responsible for triggering the

instability.

We have discovered that, in addition to the $m = 1$ mode, other higher-order modes also are allowed to come into play within a single model as long as corotation points for these modes also exist within the star. This can happen as long as the rotational profile is sufficiently steep. In our $n = 1$ polytropic neutron star models, these modes grow relatively slowly compared to previous results for softer EOSs (Centrella et al. 2001; Saijo et al. 2003), but nevertheless they appear to be dynamically unstable. Such modes are likely to develop in newly born neutron stars because young neutron stars are expected to have strong differential rotation (Ott et al. 2005b; Akiyama & Wheeler 2005). Also, because they develop in low $T/|W|$ configurations on a dynamical time scale, these modes are likely to be more important than the often-discussed secular bar-mode instability. This will have important consequences for the detection of gravitational-waves by the Laser Interferometer Gravitational-wave Observatory (LIGO), because gravitational-waves generated in such systems would not be monochromatic; our simulations indicate that signals with different characteristic frequencies are likely to peak at different times.

We suspect that these corotation-related instabilities have not been identified in previous studies of models that have a stiff EOS because earlier studies have been focused on a search for, or the analysis of, instabilities that develop on a very short time scale. Most previous simulations have been followed through only a few tens of T_c , which is not a long enough time to permit significant amplification of many of the modes we have identified in this study. Only in this study – which was initially aimed at examining the secular bar-mode instability in stars with differential rotation – have models been evolved long enough to reveal the corotation instabilities that grow on a longer time scale for this stiff EOS case.

Based on theoretical analyses of differentially rotating configurations that have been presented by others, we suspect that, in addition to the existence of corotation points, a resonant cavity is required in order to drive corotation instabilities to very large amplitude. In particular, Lovelace et al. (1999) have suggested that a local minimum in the radial vortensity profile can serve as a resonant cavity to trap waves and, hence, trigger a “Rossby wave” instability. Figures 12 and 13 display the radial vortensity profiles of our models **J068** and **J127** at different times. (The vortensity plotted here is the ratio between vorticity and volume density, but the same radial profile is preserved even if we define vortensity as the ratio between vorticity and surface density.) As these figures show, a fairly wide dip encompasses the corotation radii of all of the modes that we have found to be unstable in these models. We note that such a dip in the radial vortensity profile is a common feature for all of our unstable models. We suspect that waves are trapped inside these vortensity cavities and are continuously amplified through multiple passages across their respective corotation radii.

Because an off-axis density maximum alone will generate a vortensity minimum and hence form a resonant cavity that can trap waves inside, it is perhaps not surprising that toroidal structures frequently have been found to be unstable to a one-armed, spiral instability (Saijo et al. 2003). However, our new results show that a toroidal structure is not necessary to generate a vortensity minimum; strong differential rotation alone can create a vortensity minimum, as indicated for example by our model **J068** which does not have a toroidal structure.

We have also noticed that an unstable mode whose corotation radius falls at a position that is deeper in the vortensity well has a higher growth rate in any given simulation. Figures 12 and 13, in conjunction with the data provided in Table 2, reveal this correlation between the growth rate of each mode and the depth of its corotation radius inside the vortensity well. This correlation is consistent with the results reported by Li et al. (2000) from a study of the Rossby-wave instability in differentially rotating thin disks. They discovered that the growth rate of the Rossby-wave instability was proportional to the amplitude of density bumps/jumps that were introduced into their models, in other words, proportional to the depth of the vortensity wells that were created by such density jumps.

According to Li et al. (2000), requiring a minimum to be present in a star’s radial vortensity profile before the star can become susceptible to a corotation instability is a generalization of the Rayleigh inflexion point theorem, which states that a necessary condition for an instability of this type to develop is that there be an inflection point in the velocity profile (Drazin & Reid 1981). Given the j-constant-like rotation law (Eq. 1) adopted in our (as well as previous) studies, the condition $\partial^2 v_\phi / \partial^2 R = 0$ can be evaluated analytically to show that a velocity inflection point arises at $R = A/\sqrt{3}$. Hence, for a sufficiently shallow rotational profile having $A > \sqrt{3}R_{\text{eq}}$, the required inflection point does not exist inside the star. This may also explain why low $T/|W|$ instabilities only show up in stars with strong differential rotation (smaller values of A).

Finally, in an effort to draw a further connection between our results and previous analyses, we have examined the azimuthal structure of the unstable eigenmodes in our models. Figure 14 displays the phase angle of the $m = 1$ mode as a function of R in the equatorial plane of model **J250**. The pattern shows a slightly trailing segment in the innermost region, then transforms itself into a leading wave outside the density maximum, and finally a loosely wound, trailing segment appears again outside the corotation radius. This particular characteristic is reminiscent of the $m = 1$ structure that was observed in an earlier study of Papaloizou-Pringle modes by Woodward et. al. (1994), and it is quite similar to the azimuthal structure of the one-armed spiral mode discussed by Saijo & Yoshida (2005). In contrast, Figure 15 shows the phase-angle plot of the $m = 2$ mode for model **J068**. No

spiral structure is observed for the $m = 2$ mode; instead, the phase angles at different radii are roughly aligned along a straight line indicating a purely bar-like deformation. The radial eigenfunction of the $m = 1$ mode shown in Fig. 3 is not monotonic and has a node between the center and the surface; we suspect it belongs to the family of Papaloizou-Pringle modes that arises in pressure-supported tori and thick accretion disks. The nodeless feature of the radial eigenfunctions for $m = 2, 3$ modes suggests that they might be f-mode oscillations (this interpretation is consistent with the unstable mode structure presented by Shibata et al. (2003)); but their structures are different in details: the eigenfunction of the $m = 2$ mode (seen in **J068**) starts from zero at the center, monotonically increases outward, and reaches a maximum amplitude near the surface; in contrast, the eigenfunction of the $m = 3$ mode (seen in **J127**) has a maximum between the center and the surface.

We would like to thank Hui Li for insightful and useful discussions at the 47th Meeting of the Division of Plasma Physics of the American Physical Society. We also thank Juhan Frank, Patrick Motl, Shin Yoshida, and Christian Ott for helpful comments and suggestions. It is a pleasure to thank Anna Watts for useful conversations at the Eighth Divisional Meeting of High Energy Astrophysics Division of the American Astronomical Society. We thank an anonymous referee for helpful suggestions. This work was partially supported by NSF grants AST-0407070 and PHY-0326311. The computations were performed on the Supermike cluster and the Superhelix cluster at LSU, and on the Tungsten cluster at National Center for Supercomputing Applications (NCSA).

REFERENCES

- Akiyama, S., & Wheeler, J. C., 2005, *ApJ*, 629, 414
- Andersson, N. 2003, *Class. Quant. Grav.*, 20, 105
- Brown, J. D. 2000, *Phys. Rev. D*, 62, 084024
- Cazes, J. E., & Tohline, J. E. 2000, *ApJ*, 532, 1051
- Centrella, J. M., New, K.C.B., Lowe, L., Brown, J.D. 2001, *ApJ*, 550, L193
- Chandrasekhar, S. 1969, *Equilibrium Figures of Equilibrium*, New Haven, CT: Yale Univ. Press
- Chandrasekhar, S. 1970, *ApJ*, 161, 561
- Drazin, P. G., & Reid, W. H., *Hydrodynamic Stability* (Cambridge: Cambridge Univ. Press)

- Durisen, R. H., Gingold, R. A., Tohline, J. E., & Boss, A. P. 1986, *ApJ*, 305, 281
- Frank, J., & Robertson, J.A., 1988, *MNRAS*, 232, 1
- Friedman, J., & Schutz, B. F. 1978, *ApJ*, 222, 281
- Goldreich, P., Goodman, J., & Narayan, R., 1986, *MNRAS*, 221, 339
- Hachisu, I. 1986, *ApJS*, 61, 479
- Ipsier, J. R., & Lindblom, L. 1990, *ApJ*, 355, 226
- Ipsier, J. R., & Lindblom, L. 1991, *ApJ*, 373, 213
- Lai, D., & Shapiro, S. L. 1995, *ApJ*, 442, 259
- Li, H., Finn, J. M., Lovelace, R. V. E., & Colgate, S. A., 2000, *ApJ*, 533, 1023
- Li, H., Colgate, S. A., Wendroff, B., Liska, R., 2001, *ApJ*, 551, 874
- Liu, Y. T., 2002, *Phys. Rev. D*, 65, 124003
- Lovelace, R. V. E., Hohlfield, R. G., 1978, *ApJ*, 221, 51
- Lovelace, R. V. E., Li, H., Colgate, S. A., Nelson, A. F., 1999, *ApJ*, 513, 805
- Motl, P. M., Tohline, J. E., & Frank, J. 2002, *ApJS*, 138, 121
- Narayan, R., Goldreich, P., & Goodman, J., 1987, *MNRAS*, 228, 1
- New, K. C. B., Centrella, J. M., & Tohline, J. E. 2000, *Phys. Rev. D*, 62, 064019
- Ott, C. D., Burrows, A., Livne, E., & Walder, R. 2004, *ApJ*, 600, 834
- Ott, C.D., Ou, S., Tohline, J.E., Burrows, A., 2005a, *ApJ*, 625, L119
- Ott, C. D., Burrows, A., Thompson, T. A., Livne, E., & Walder, R. 2005b, *astro-ph/0508462*
- Ou, S., ,Tohline, J.E, Lindblom, L. 2004, *ApJ*, 617, 490
- Papaloizou, J.C.B., Pringle, J.E., 1984, *MNRAS*, 208, 721
- Papaloizou, J.C.B., Lin, D. N. C., 1989, *ApJ*, 344, 645
- Saijo, M., Baumgarte, T. W., & Shapiro, S. L. 2003, *ApJ*, 595, 352
- Saijo, M., & Yoshida, S., 2005, *astro-ph/0505543*

- Shibata, M., & Karino, S. 2004, Phys. Rev. D, in press (astro-ph/0408016)
- Shibata, M., Karino, S., & Eriguchi, Y. 2002, MNRAS, 334,L27
- Shibata, M., Karino, S., & Eriguchi, Y. 2003, MNRAS, 343, 619
- Tassoul, J.-L. 1978, Theory of Rotating Stars, Princeton: Princeton University Press
- Tohline, J. E., Durisen, R. H., & McCollough, M. 1985, ApJ, 298, 220
- Tohline, J. E., Hachisu, I., 1990, ApJ, 361, 394
- Watts, A. L., Andersson, N., & Jones, D. I. 2005, ApJ, 618, L37
- Williams, H. A., & Tohline, J. E. 1988, ApJ, 334, 449
- Woodward, J. W., Tohline, J. E., & Hachisu, I., 1988 ApJ, 420, 247

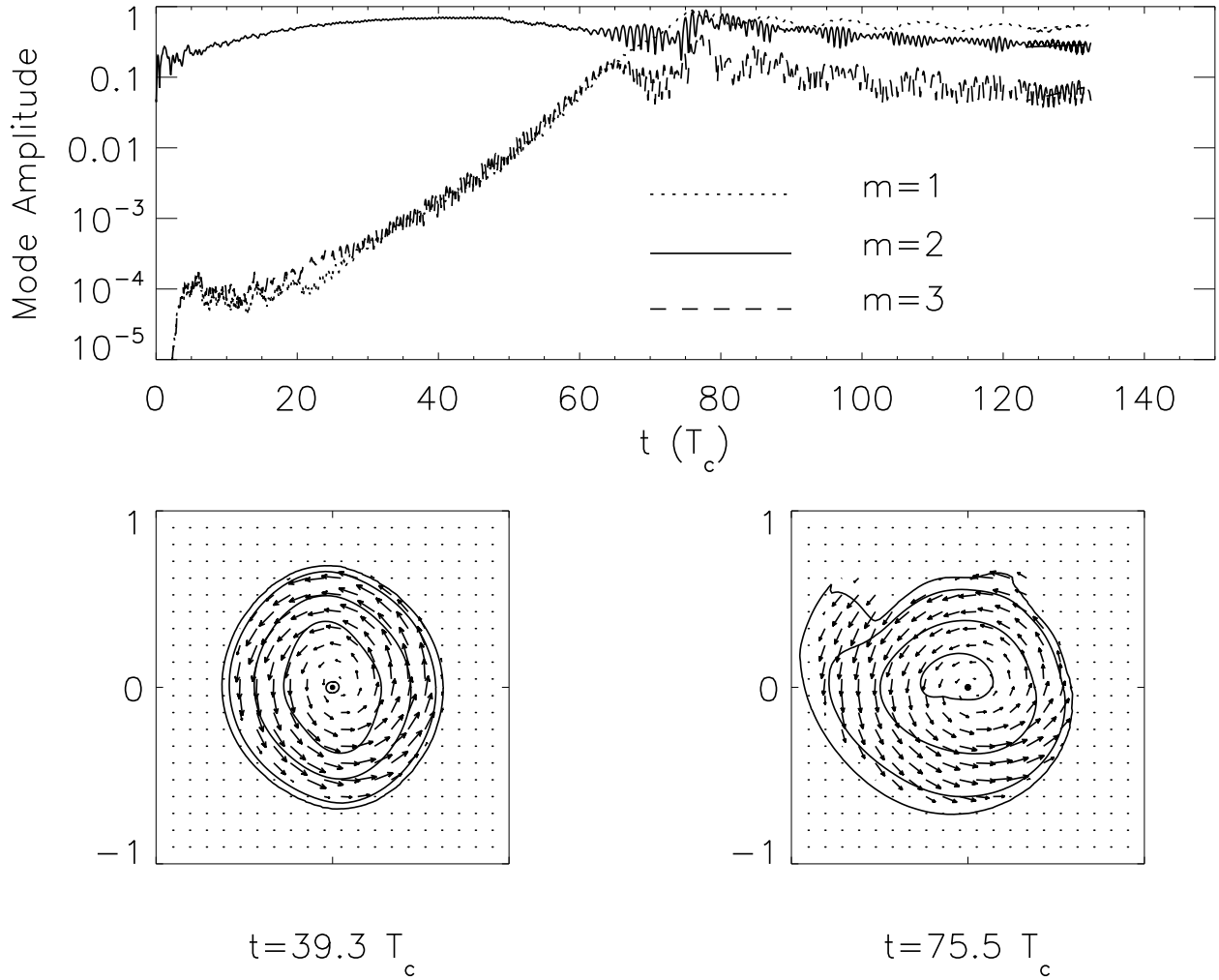


Fig. 1.— The top panel shows $m = 1, 2,$ and 3 Fourier amplitudes as a function of time t in the equatorial plane of model **J250** when GRR was turned on; t is normalized to the central spin period T_c of the differentially rotating star. The bottom panels show equatorial-plane isodensity contours at two different evolutionary times, with inertial-frame velocity vectors superposed; contour levels are (from the innermost, outward) $\rho/\rho_{\max} = 0.9, 0.5, 0.1,$ and 0.01 .

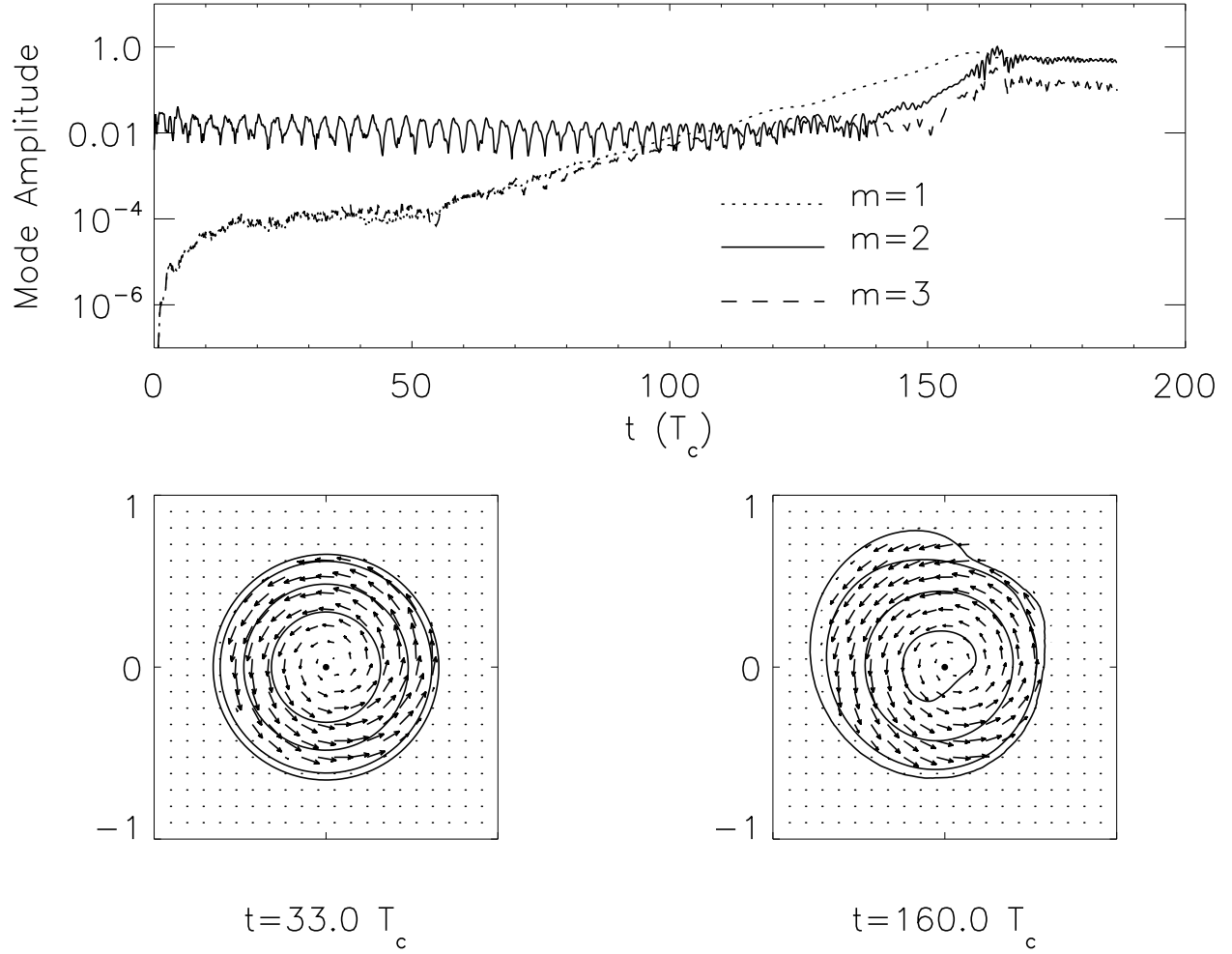


Fig. 2.— Same as Figure 1, but for model **J250** when GRR forces are turned off.

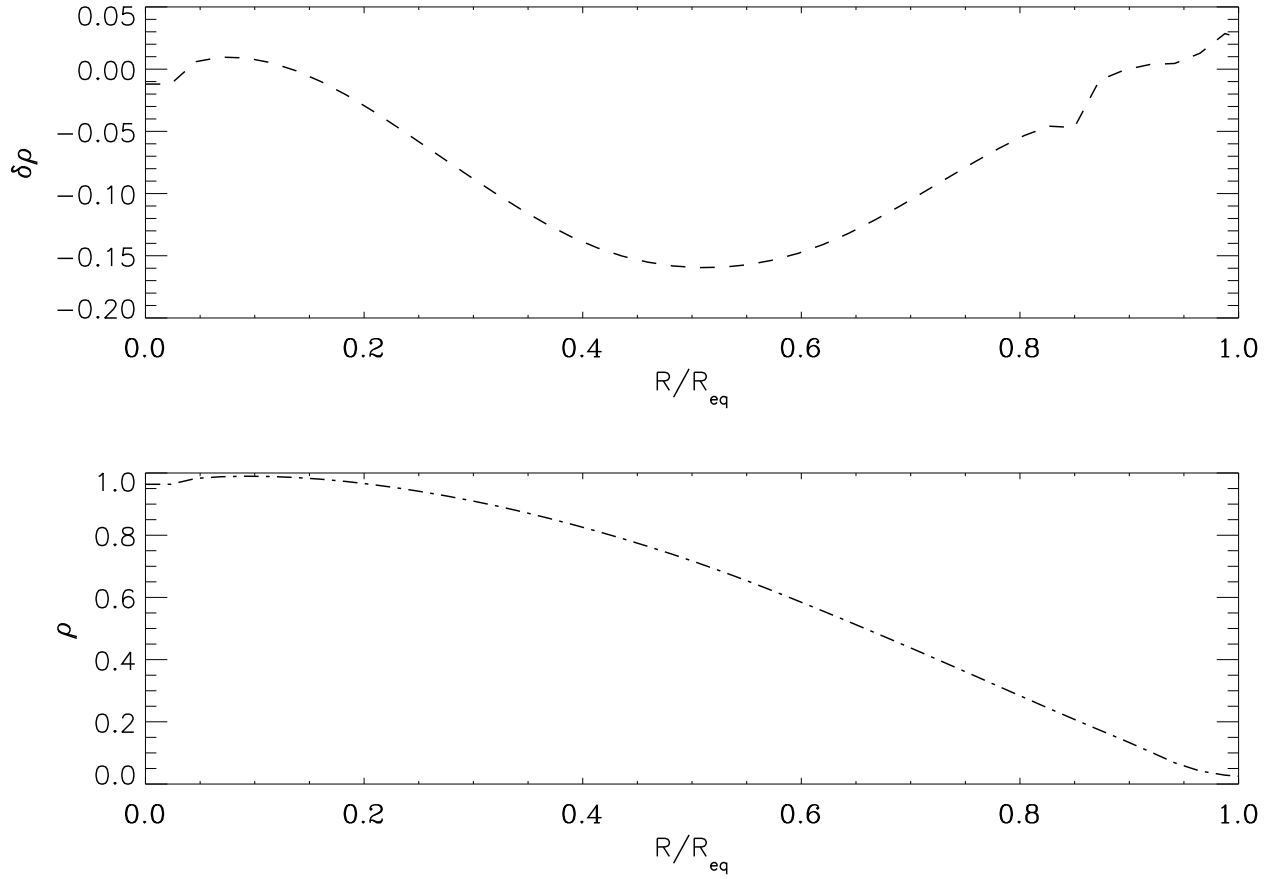


Fig. 3.— The top and bottom panels show, respectively, $\delta\rho(R)$ and $\rho(R)$ for model **J250** in the equatorial plane when the $m = 1$ mode is dominant.

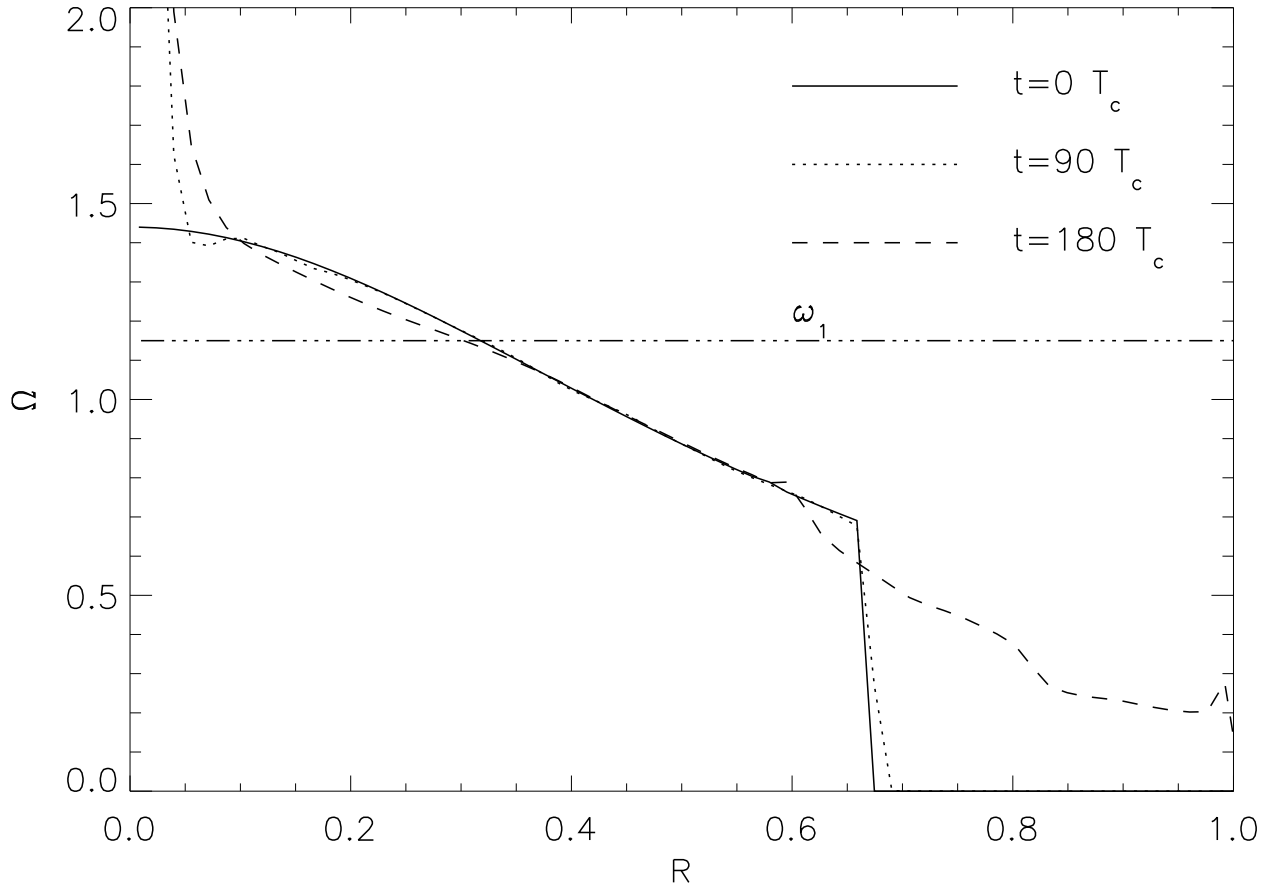


Fig. 4.— The rotational profile $\Omega(R)$ of model **J250** is shown at three different evolutionary times. The dash-dotted horizontal line identifies the measured eigenfrequency ω_1 of the unstable $m=1$ mode.

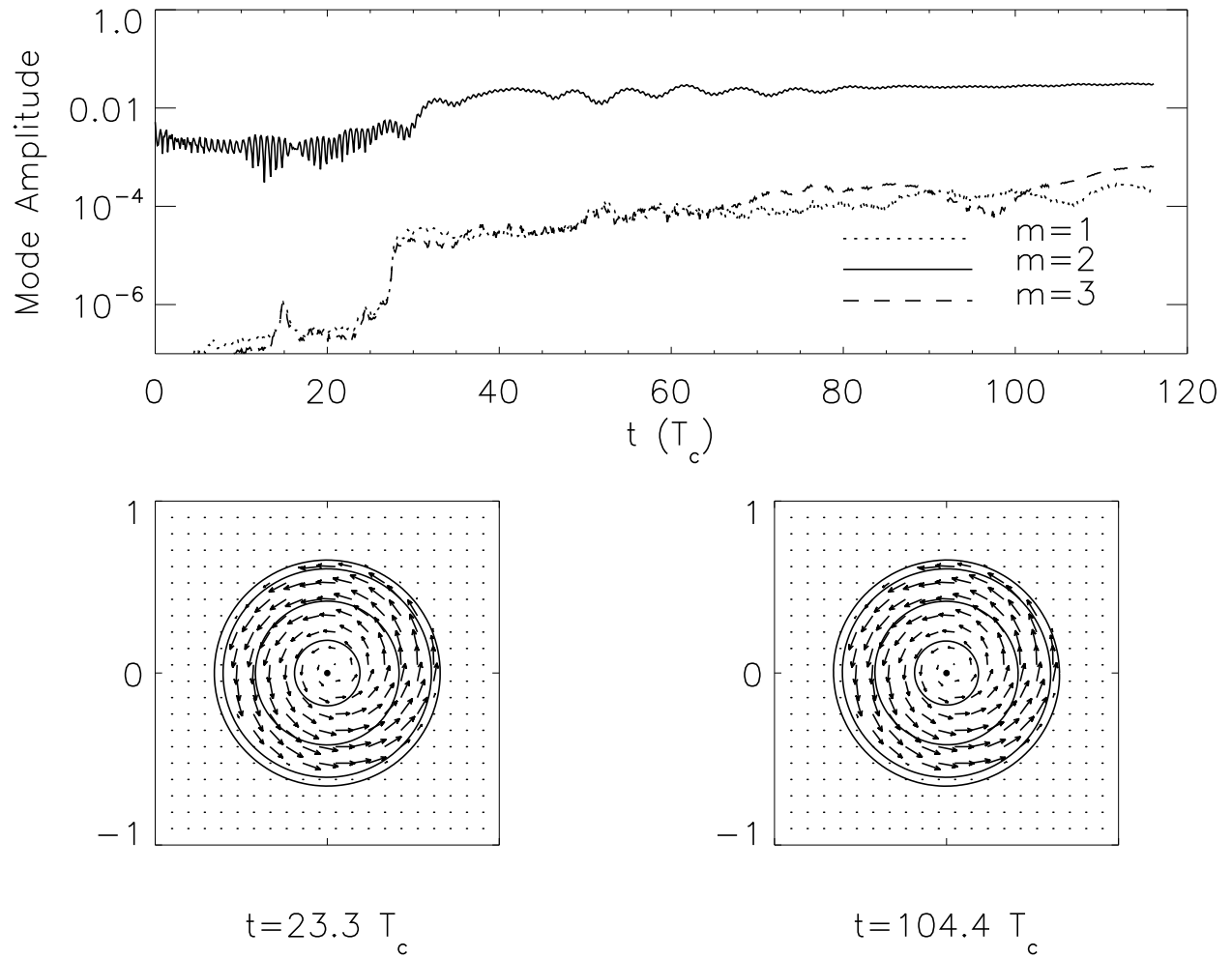


Fig. 5.— Same as Fig. 1, but for model **J133** when GRR forces are turned off.

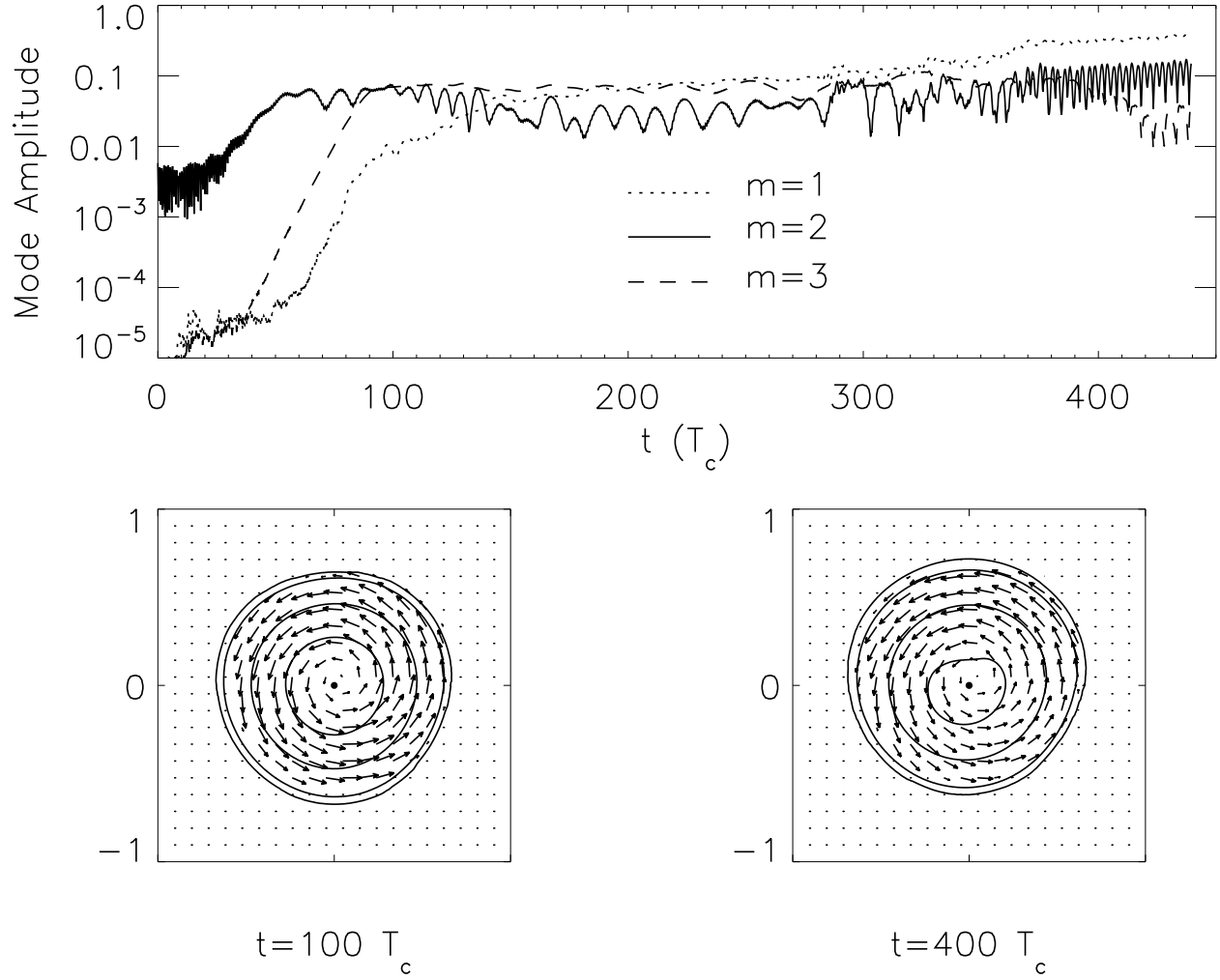


Fig. 6.— The same as Figure 1, but for model **J127** with GRR turned off.

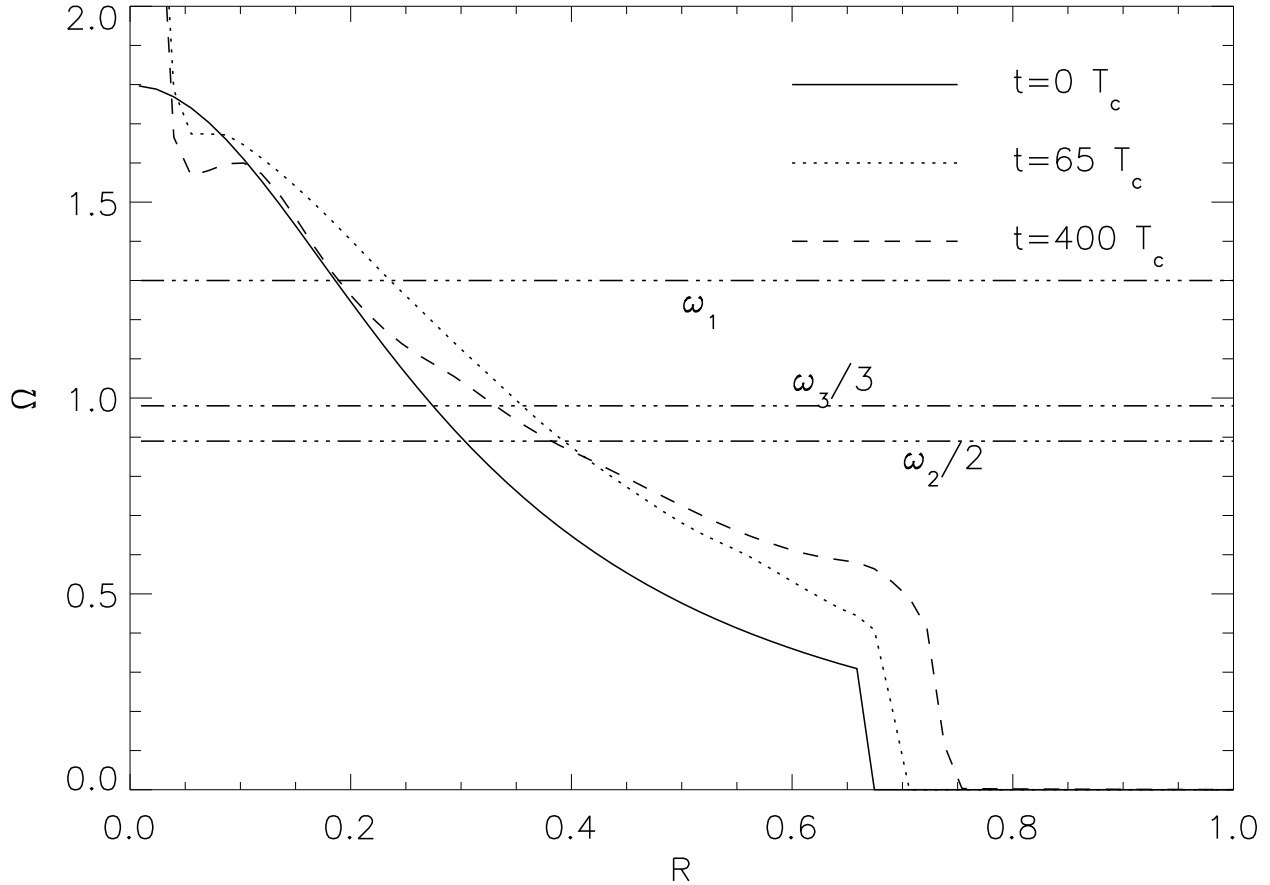


Fig. 7.— The angular velocity profile $\Omega(R)$ is shown for model **J127** at three different evolutionary times. Dash-dotted horizontal lines denote the measured eigenfrequencies ω_1 , ω_2 and ω_3 of various unstable modes. $\omega_2/2$ is measured at $\sim 50 T_c$, $\omega_3/3$ is measured at $\sim 80 T_c$, and ω_1 is measured at $\sim 400 T_c$. To determine a corotation radius, we used a rotational profile that is around at the same time when each frequency is measured.

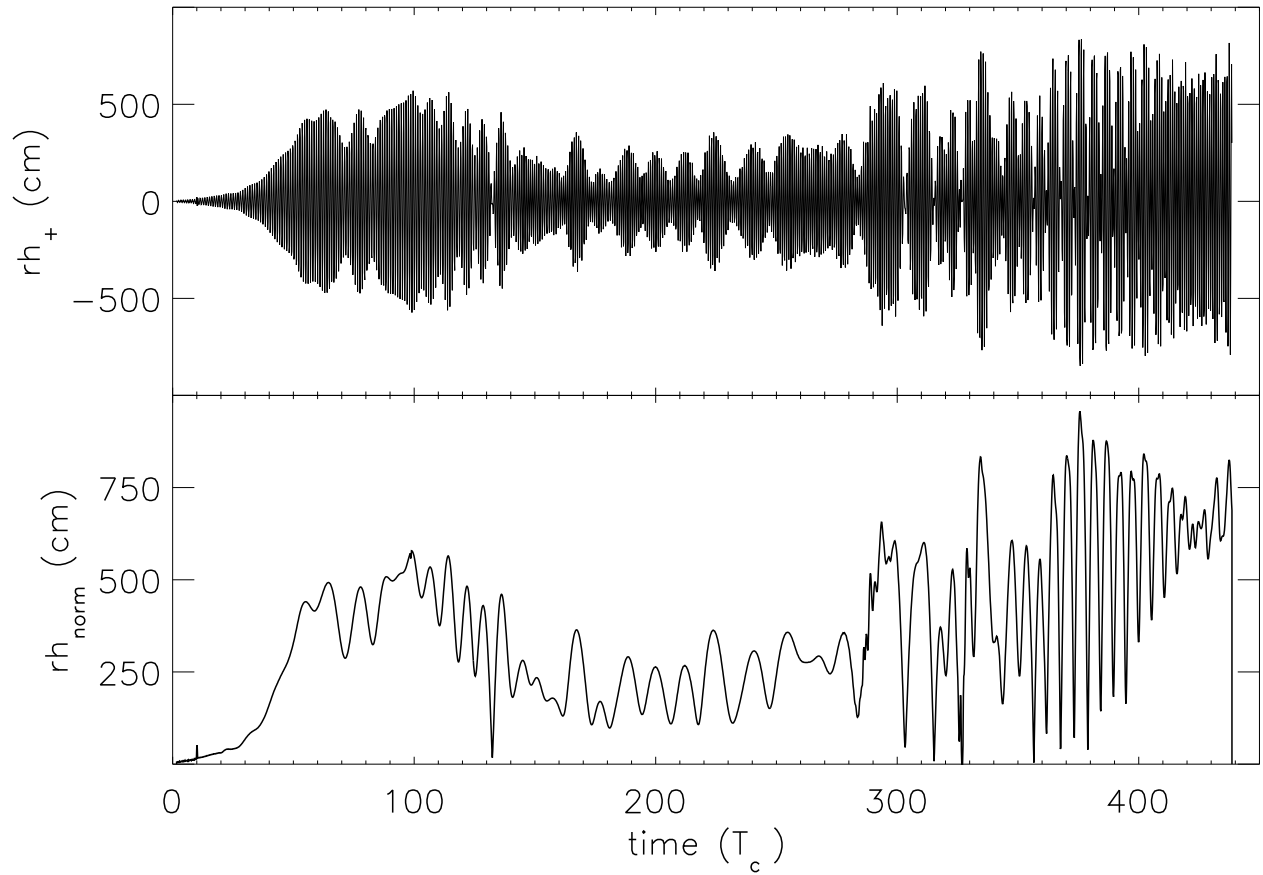


Fig. 8.— The quadrupole gravitational-wave strain that would be radiated from model **J127** as viewed by an observer looking down the Z (rotation) axis.

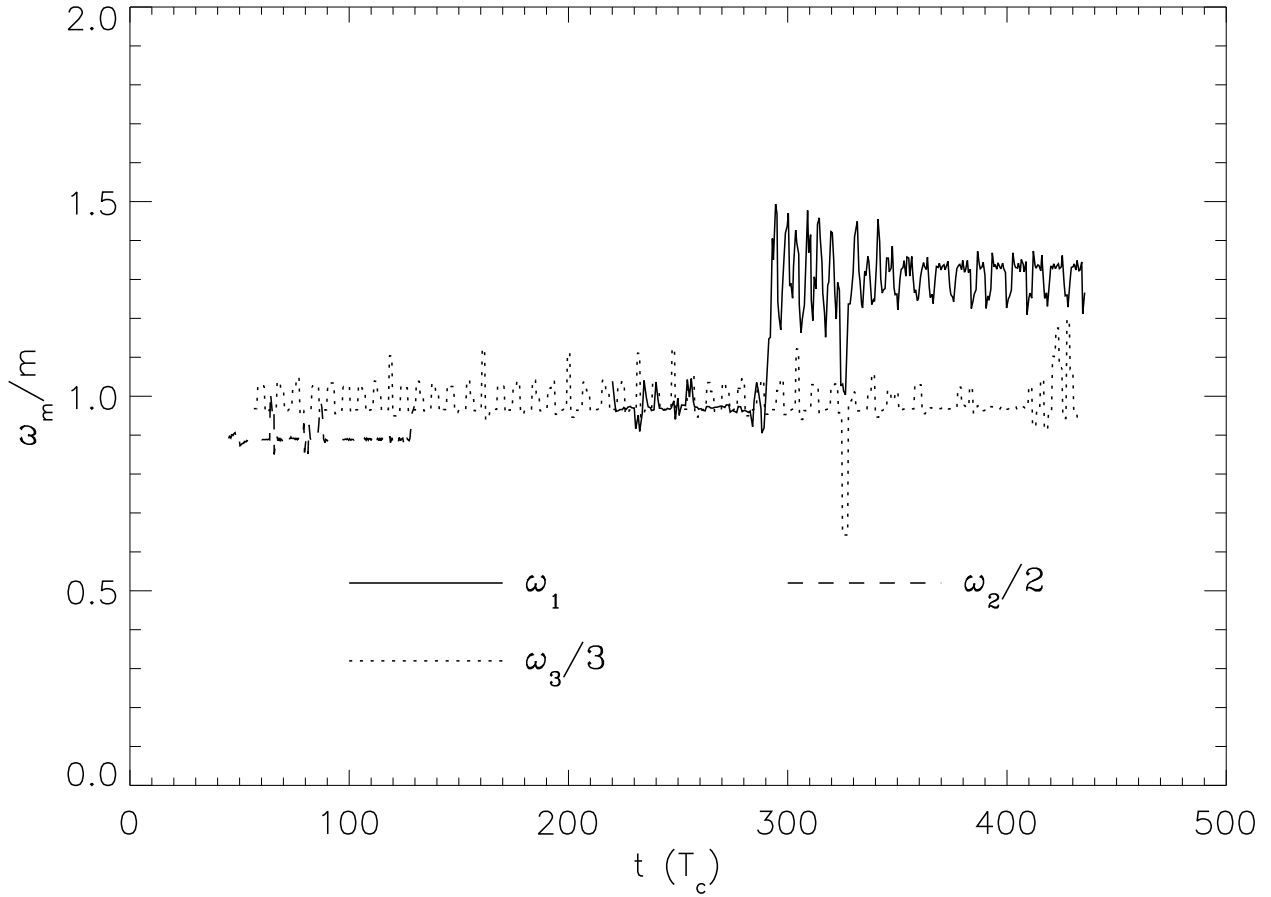


Fig. 9.— The pattern frequencies of different modes is displayed as a function of time for model **J127**. The frequency $\omega_2/2$ is measured between 40 and 130 T_c , $\omega_3/3$ is measured between 50 and 430 T_c , and ω_1 is measured between 220 and 430 T_c .

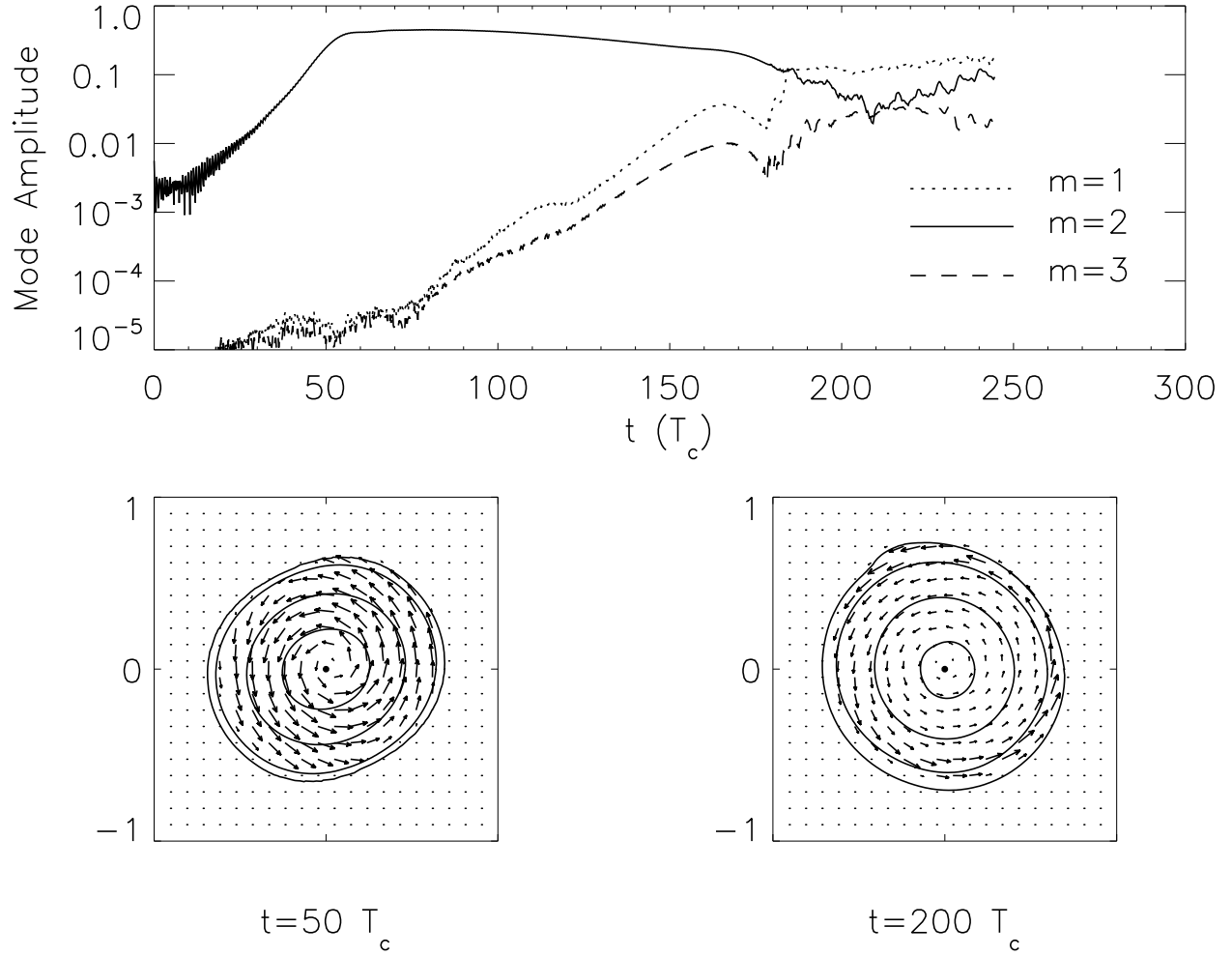


Fig. 10.— Same as Figure 1, but for model **J068** when GRR is turned off.

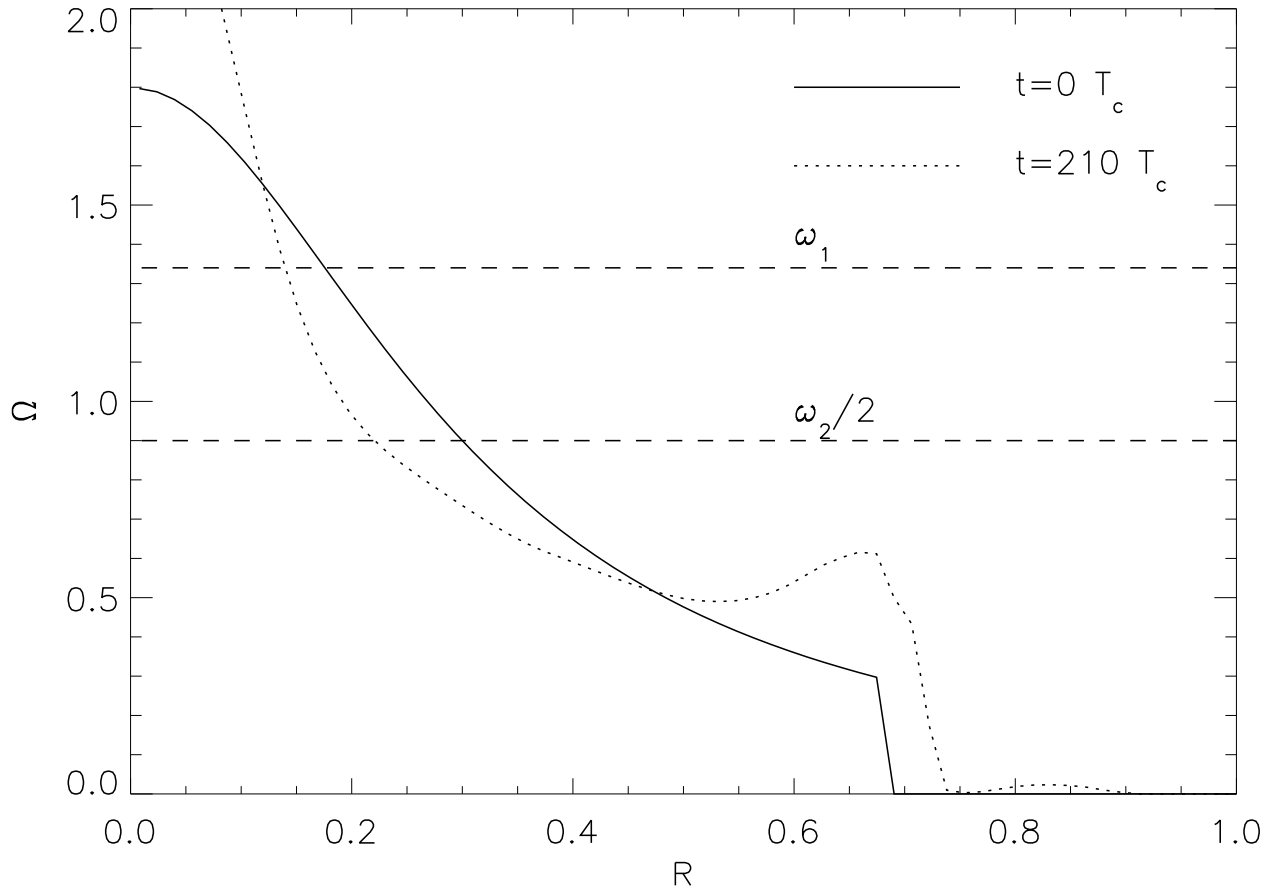


Fig. 11.— The angular velocity profile $\Omega(R)$ of model **J068** is plotted at two different times during its evolution. Dashed horizontal lines identify measured eigenfrequencies of the unstable $m = 1$ and $m = 2$ modes.

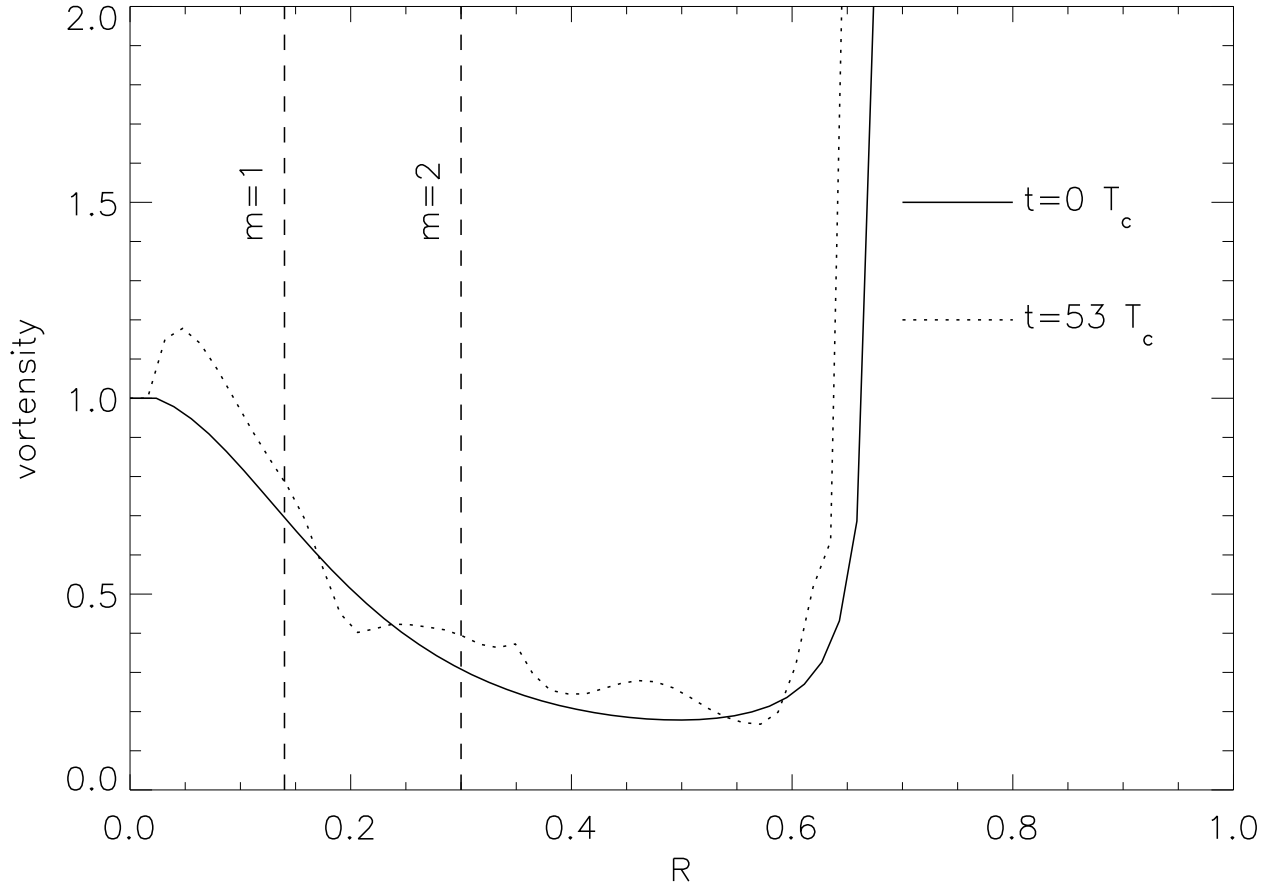


Fig. 12.— The radial vortensity profile is shown for model **J068** initially (solid line) and at a time $t = 53T_c$ (dotted line) during its evolution. The horizontal axis is the cylindrical radius, the vertical axis is the vortensity normalized to the value on the Z axis. The two vertical dashed lines locate the corotation radii for $m = 1$ (left) and $m = 2$ (right) modes. There seems to be a correlation between the growth rate and the location of corotation radii inside the vortensity well: the $m = 2$ mode with a “deeper” corotation radius in the initial vortensity well was the first unstable mode to arise in the simulation, whereas the $m = 1$ mode whose corotation radius lies at a “shallower” location in the initial vortensity well developed later in the evolution.

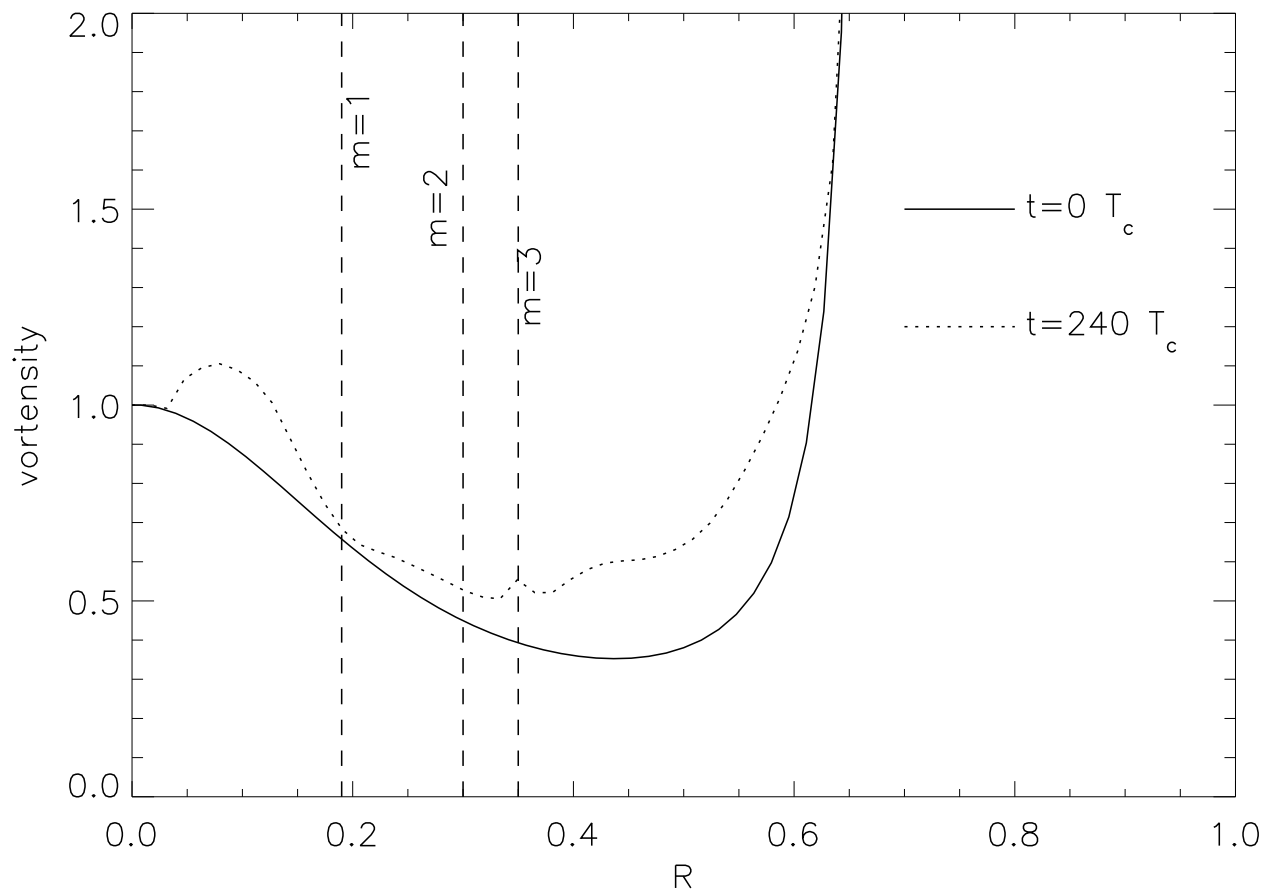


Fig. 13.— The radial vortensity profile is shown for model **J127** initially (solid line) and at a time $t = 240T_c$ (dotted line) during its evolution. The horizontal axis is the cylindrical radius, the vertical axis is the vortensity normalized to the value on the Z axis. The three vertical dashed lines locate the corotation radii for $m = 1$ (left), $m = 2$ (middle), and $m = 3$ (right) modes.

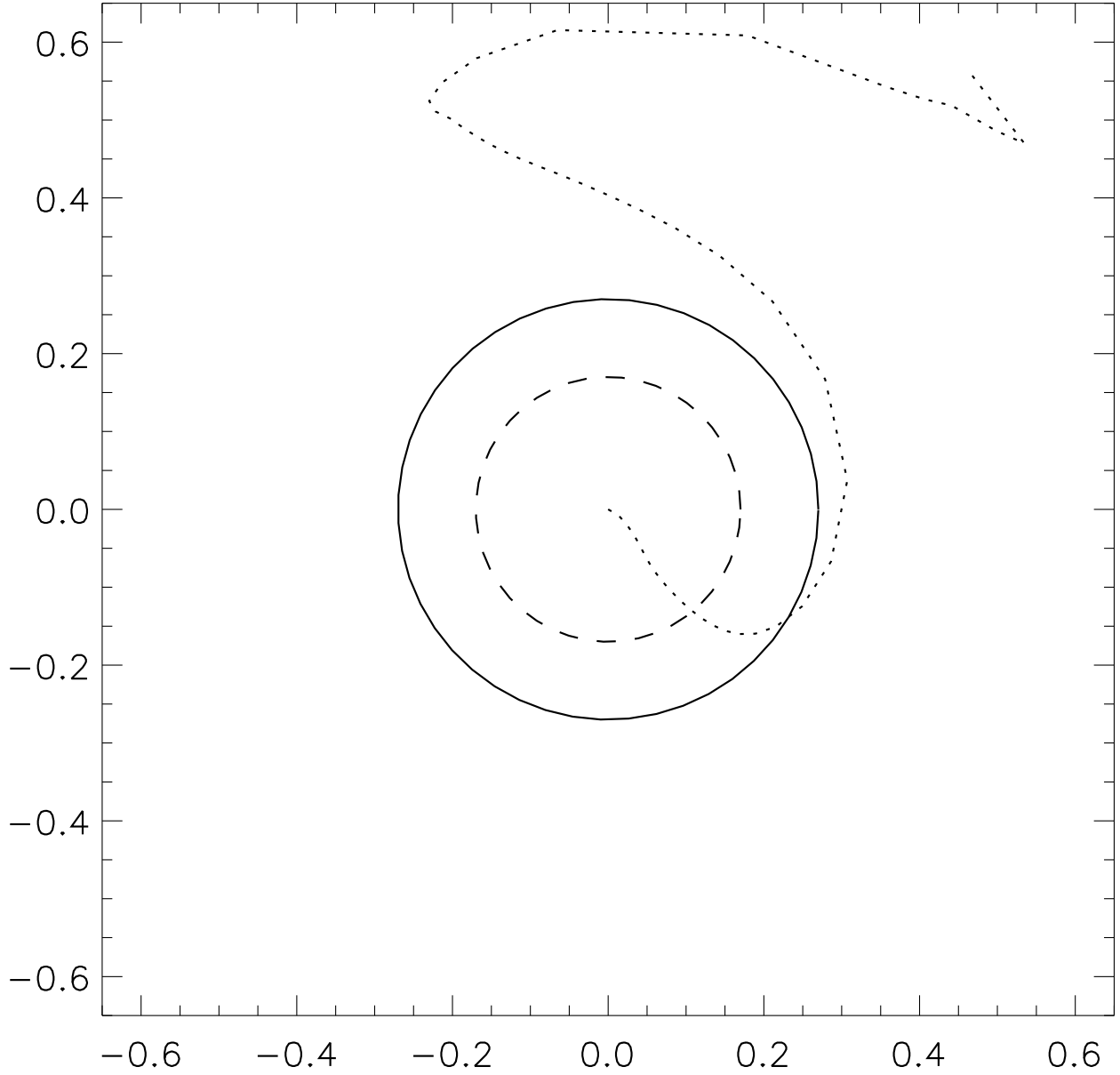


Fig. 14.— The dotted curve displays the azimuthal structure $\phi_1(R)$ of the $m = 1$ eigenfunction in the equatorial plane of model **J250** at $t = 95.4T_c$ when GRR was turned on. The solid circle denotes the corotation radius; the dashed circle denotes the location of density maximum.

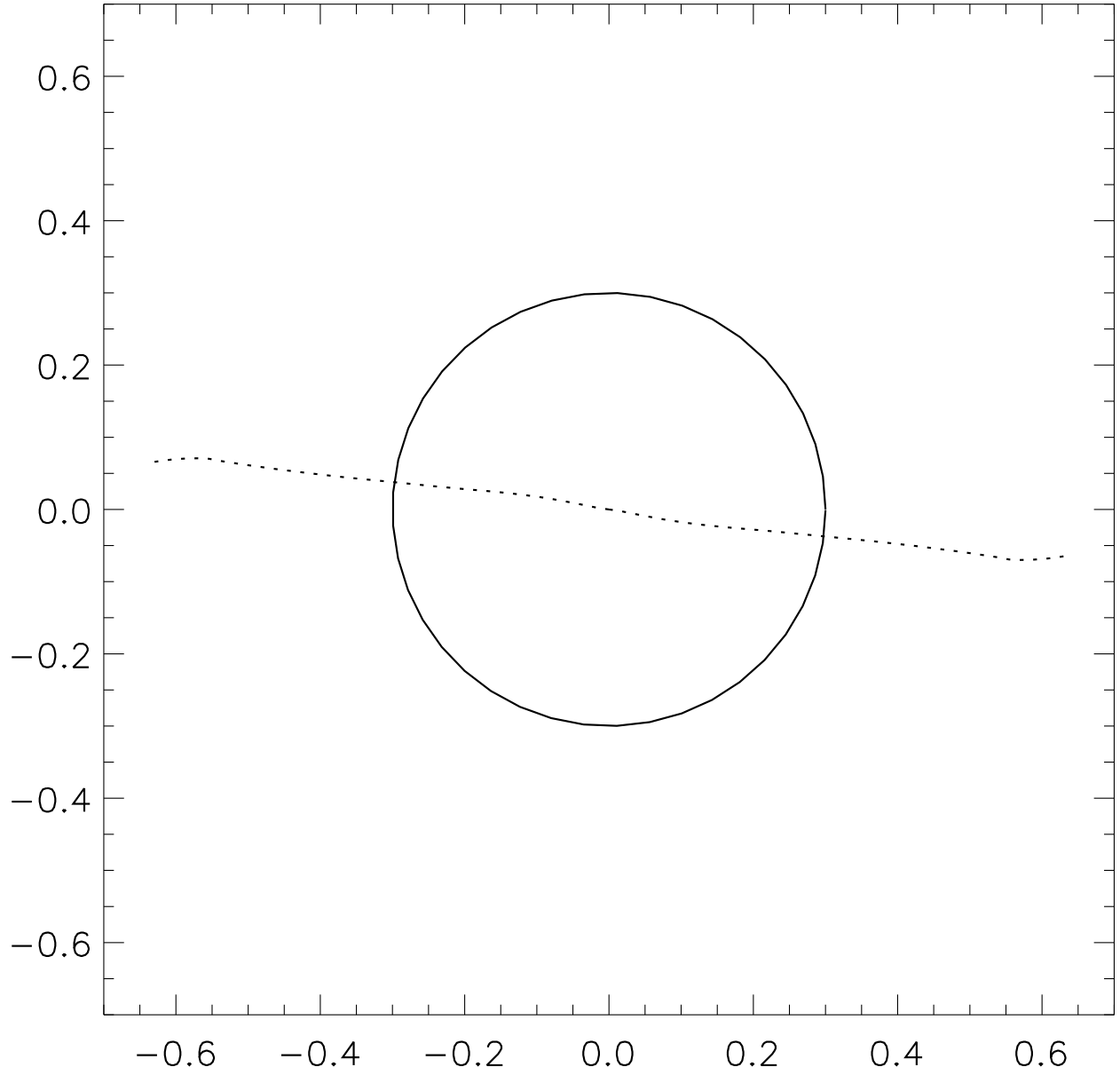


Fig. 15.— Same as Figure 14 but for the $m = 2$ mode of model **J068** when $t = 70T_c$; there is no dashed circle because the density maximum lies at the center of the star.